Current Chemistry Letters 15 (2026) 871–882

Contents lists available at GrowingScience

Current Chemistry Letters

homepage: www.GrowingScience.com

Eco-friendly removal of heavy metals using Moroccan calcite-quartz clay: Adsorption performance and mechanistic insights

Zineb El Kerdoudi[a], Othmane Hammani[b], Abdelhadi El Rhilassi[a,c*], Jaouad Bensalah[d] and Nouredine El Mejdoub[a]

[a]*Laboratory of Organic chemistry, catalysis, and environment (LOCCE), Department of Chemistry, Faculty of Sciences, Ibn Tofaïl University, B.P. 133, 14000 Kenitra, Morocco*
[b]*National Center for Scientific and Technical Research (CNRST), Rabat, Morocco*
[c]*Training Center of Education Inspectors (CFIE) of Rabat, Morocco*
[d]*Laboratory of Advanced Materials and Process Engineering (LAMPE), Department of Chemistry, Faculty of Sciences, Ibn Tofaïl University, B.P. 133, 14000 Kenitra, Morocco*

C H R O N I C L E

Article history:
Received January 25, 2026
Received in revised form
March 25, 2026
Accepted June 25, 2026
Available online
June 25, 2026

Keywords:
Calcite-quartz clay
Heavy metal adsorption
Adsorption
Wastewater treatment
Natural adsorbent

A B S T R A C T

The treatment of water polluted by harmful metals such as zinc and copper is a major challenge due to its consequences for the environment and health. This study examines the potential of a calcite-quartz clay from western Morocco as an abundant, inexpensive, and effective adsorbent for their removal. The adsorption mechanisms were elucidated using kinetic and isothermal modeling, supported by an in-depth physicochemical and structural characterization of the adsorbent, including X-ray fluorescence, X-ray diffraction, Fourier-transform infrared spectroscopy, thermal analysis, scanning electron microscopy coupled with energy-dispersive X-ray spectroscopy, and textural characterization by specific surface area measurement. The kinetics, which follow the pseudo-second order model, are both rapid and efficient. For Zn^{2+} (10 mg. L^{-1}, pH= 6.5), equilibrium is reached in 120 minutes, with a maximum capacity of 61.22 $mg.g^{-1}$ and a removal rate of 99.46 %. Cu^{2+} (pH=5.6) shows comparable behavior, with stabilization at 150 minutes, a capacity of 59.40 $mg.g^{-1}$ and an efficiency of 91.46 %. Analysis of the isotherms shows that the adsorption of Cu^{2+} by the clay under study follows the Langmuir model, whereas the adsorption of Zn^{2+} exhibits behavior consistent with adsorption at multiple sites, in accordance with the Freundlich model. SEM-EDX and FTIR analyses confirmed the adsorption of the metals studied at the clay interface. These results highlight the validity and importance of the calcite-quartz clay analyzed for the treatment of effluents loaded with copper and zinc, offering a favorable alternative to traditional methods.

2026 by the authors; licensee Growing Science, Canada.

1. Introduction

The development of the industrial sector, especially in the fields of metallurgy, surface treatment and the chemical industry in Morocco, has been accompanied by a sharp increase in the volume of liquid waste contaminated with heavy metals[1]. Zinc and copper are among these pollutants and they are an important source of environmental problems[2]. Furthermore, these heavy metals are not biodegradable and persist in the environment; they are toxic even at extremely low concentrations. These substances are harmful to aquatic ecosystems, accumulate in the food chain, and can cause serious kidney, neurological, and cancer-related diseases in humans[3]. Due to these risks, international organizations are imposing increasingly strict discharge standards, which requires the development of effective, cost-efficient and environmentally friendly treatment technologies. Several wastewater treatment processes are used to remove heavy metals such as precipitation[4], ion exchange[5], membrane filtration[6], and adsorption[7]. Indeed, adsorption remains one of the most promising methods due to its ease of use, low cost and effectiveness. The adsorbents studied are numerous and varied such as activated carbon[8], zeolites[9], and clays[10]. Clays are among the materials attracting growing interest due to their remarkable

* Corresponding author Tel : +212 6 62 13 13 72
E-mail address aelrhilassi@gmail.com (A. El Rhilassi)
© 2026 by the authors; licensee Growing Science, Canada
doi: 10.5267/j.ccl.2026.6.009

physicochemical properties, namely their high cation exchange capacity, their large specific surface area, and their abundance in nature. Many studies have been published on the removal of heavy metals by clays but few have been devoted to the use of natural Moroccan clays, especially those rich in calcite and quartz, as low-cost adsorbents for the treatment of polluted waters. The detailed characterization of these materials and the assessment of their adsorption performance are still insufficiently documented in the scientific literature. In this sense, the objective of the present work is to evaluate the potential of a natural Moroccan clay, from the region of Sidi Kacem, mainly composed of calcite and quartz, for the removal of zinc and copper from aqueous solutions. The approach includes a complete physicochemical and mineralogical characterization of the material, the study of the effect of the main operating parameters (dose of adsorbent, contact time, initial concentration and temperature) on the adsorption, as well as the kinetic and thermodynamic modeling of the process.

The results obtained will provide a better understanding of the adsorption mechanisms involved and demonstrate the suitability of this natural, locally available, and abundant material as an environmentally friendly and cost-effective alternative for wastewater treatment in Morocco.

2. Materials and methods

2.1 Protocol for preparing the adsorbent

The calcite-quartz clay studied comes from a region near the Oued Ouargha, specifically from Khenichet (Morocco). The sample was ground into a powder, then sieved (particle size ≤ 56 micrometers), and dried at a temperature of 105 °C for 24 hours, before being stored in a dry environment for analysis, in accordance with a standard protocol.

2.2 Zn^{2+}/Cu^{2+} metal solution

Using $ZnSO_4.7H_2O$ and $CuSO_4.5H_2O$, we prepared stock solutions of zinc and copper at a concentration of 1 g/L. These were then diluted as needed to obtain working solutions for each element, with concentrations ranging from 10 to 200 mg/L.

2.3 Experimental study

2.3.1 Adsorption kinetics of heavy metals on calcite-quartz clay

Zn^{2+} and Cu^{2+} ion adsorption tests were performed in batch mode at a controlled temperature. For each experiment, 15 mg of calcite-quartz clay was exposed to 100 mL of a solution containing the analyzed metal at an initial concentration of 10 $mg.L^{-1}$, while maintaining constant agitation. The solid and liquid phases were separated by centrifugation at 3000 rpm for five minutes after the 180-minute contact period. The residual metal content in the supernatant was then measured by inductively coupled plasma mass spectrometry (ICP-OES)[11].

2.4 Modeling adsorption isotherms

Data processing and adjustment of theoretical models to experimental results were performed using OriginPro 2018 software. The most representative adsorption model was selected by favoring the one with the highest coefficient of determination (R^2) and the closest agreement between calculated values and measured data, as shown in the results tables.

2.5 Adsorption kinetics

The batch adsorption process consists of bringing a given mass of solid adsorbent (m) into contact with a volume (V) of solution containing the contaminant at an initial concentration (C_i). At equilibrium, the residual concentration in the solution is denoted (C_e)[12].

The adsorption capacity (q_e) represents the amount of metal retained per unit mass of adsorbent at equilibrium. It is calculated using the following mass balance equation:

$$q_e(mg/g) = V(C_i - C_e)/m \quad (1)$$

The efficiency of the process, expressed as the removal rate (R%), is determined by the following relationship:

$$R\ (\%)\ = 100 \times (C_i - C_e)/C_i \quad (2)$$

where *m(g)* is the adsorbent mass, *V(L)* is the volume of solution, C_i *(mg.L^{-1})* is the initial concentration and C_e*(mg.L^{-1})* is the equilibrium concentration.

2.5.1 Kinetic modeling: first- and second-order approaches

The kinetic data were analyzed to verify their compliance with first-order models (Lagrange equation, Eq.3) and second-order models (Eq.4).

Pseudo-first-order model:

$$ln(q_e - q_t) = ln\, q_e - K_1 t \quad (3)$$

where qt and qe are the quantities adsorbed at time t and at equilibrium (mg/g), and k1 is the rate constant (min^{-1}).

Pseudo-second-order model:

$$\frac{t}{q_t} = \frac{1}{K_2 {q_e}^2} + \frac{t}{q_e} \quad (4)$$

where k_2 is the velocity constant (g/mg·min). Linear or nonlinear adjustment of these models to the data allows the order of the adsorption reaction to be identified and information about its mechanism to be deduced[13].

2.5.2 Application of the Elovich model to adsorption kinetics

The study of chemisorption on heterogeneous surfaces was carried out using this Elovich model[14]. This model is based on the assumption of an exponential variation in activation energy with the amount adsorbed, accounting for the nonlinear kinetics characteristic of energetically different adsorption sites. The integrated kinetic equation of the Elovich model is classically expressed as[15] :

$$q_t = \frac{1}{\beta} ln(\alpha\beta) + \frac{1}{\beta} ln(t) \quad (5)$$

where q_t *(mg·g⁻¹)* is the quantity adsorbed at time t, α*(mg·g⁻¹·min⁻¹)* is the initial adsorption rate constant, β *(g·mg⁻¹)* is the parameter related to surface energy, and *t (min)* is time.

2.6 Adsorption mechanism modeling

2.6.1 Langmuir model

The Langmuir model assumes reversible adsorption in a monomolecular layer on a surface consisting of identical and energetically equivalent sites, with no lateral interaction between the adsorbed molecules[16]. It is expressed in the following linearized form:

$$\frac{C_e}{q_e} = \frac{1}{K_L\, q_m} + \frac{C_e}{q_m} \quad (6)$$

where *Ce(mg·L⁻¹)* is the equilibrium concentration, q_e*(mg·g⁻¹)* is the amount adsorbed at equilibrium, q_m *(mg·g⁻¹)* the maximum adsorption capacity of the monolayer, and k_L*(L·mg⁻¹)* Langmuir constant related to adsorption energy.

2.6.2 Freundlich model

Unlike Langmuir, Freundlich's empirical model applies to heterogeneous surfaces and describes multilayer adsorption[17]. Its linearized equation is:

$$Ln\, q_e = Ln\, k_F + \frac{1}{n}\, Ln\, C_e \quad (7)$$

where k_F *(mg¹⁻ⁿ·Lⁿ·g⁻¹)* is a constant indicative of adsorption capacity, and *n* (dimensionless) a heterogeneity factor. A value of *1/n* between 0 and 1 indicates favorable adsorption and a heterogeneous surface.

2.6.3 Temkin model

Temkin's model takes into account the interactions between the adsorbate and the adsorbent [17]. Expressed by:

$$q_e = \frac{RT}{b} ln(K_T\, C_e) \quad (8)$$

where q_e *(mg.g⁻¹)* is the quantity adsorbed at equilibrium, *b (J. mole⁻¹)*is the Temkin energy parameter, K_T *(L. mg⁻¹)* is the Temkin constant, *R (8,314 J.mol⁻¹. K⁻¹)* is the ideal gas constant, and *T (K)* is the absolute temperature.

2.7 Thermodynamic study

The thermodynamic analysis was performed using the Van't Hoff method. The standard enthalpy of adsorption (ΔH°) was calculated from the slope of the line obtained by linear regression of ln(Kc) as a function of 1/T[18].

$$Log\, K_c = \frac{\Delta S^\circ}{R} - \frac{\Delta H^\circ}{RT} \quad (9)$$

where $K_c = \frac{C_0 - C_e}{C_e}$ is the adsorption equilibrium constant, $\Delta H°$ *(cal. mol^{-1})* is the standard enthalpy of adsorption (*R* in *cal. K^{-1}. mol^{-1}*), $\Delta S°$ *(cal. mol^{-1}. K)* is the standard entropy variation, C_0 *(mg. L^{-1})* is the initial concentration, *Ce (mg. L^{-1})* is the equilibrium concentration, and *T (K)* is the absolute temperature.

2.8 Method for characterizing calcite-quartz clay

2.8.1 Fourier Transform Infrared (FTIR) Spectroscopy

Fourier transform infrared spectroscopy (FTIR) was used to identify the carbonates, organic matter, and functional groups in the clay and to characterize any potential chemical changes. The spectra, which had a resolution of 4 cm^{-1} and a range of 400 to 4000 cm^{-1}[19], were obtained using a BRUKER spectrometer at the University Center for Analysis, Expertise, Technology Transfer, and Incubation at Ibn Tofail University.

2.8.2 SEM-EDX analysis

The appearance and surface of the sample, both before and after testing, were examined using a field-emission scanning electron microscope equipped with an EDX detector. This technique allows the texture and shape of materials to be analyzed at the micro and nanometric scales, achieving a high level of magnification [20].

2.8.3 DTA-TGA analysis

The thermal stability of the clay was studied by differential thermal analysis and thermogravimetric analysis (TGA-DTA) using an SDT Q600 device (TA Instruments). The measurements were performed in air on a 100 mg sample heated from 30 to 1200 °C at a rate of 5 °C/min [21]. It allows for the study of physical and chemical changes, as well as changes in the sample's mass, as a function of temperature.

3. Results and discussion

3.1 Characterization of calcite-quartz clay before adsorption

3.1.1 X-ray Fluorescence analysis

The chemical composition of the clay under study was analyzed using X-ray fluorescence. **Table 1** lists the chemical elements contained in this clay. In the clay studied, silicon dioxide (SiO_2) is the main component (36.76 %). The presence of free silica explains this proportion. Aluminum oxide accounts for 11.33 %. As for calcium oxide, it is present in significant quantities: 17.20 %, indicating the presence of carbonates in this clay. The percentage of iron oxide is 4.40 %. This explains why this clay contains Si, Fe, Al, and Ca.

Table 1 also shows the loss on ignition associated with the heat treatment of the clay sample under study. The sample is heated to a temperature of 950 °C to induce a series of physical and chemical reactions within it. This parameter is used as a criterion for determining the organic matter and carbonate content of a material. The highest loss on ignition values were measured for calcite-quartz clay, at 20.51%.

Table 1. Chemical composition of the clay used.

Compound	SiO_2	Al_2O_3	CaO	Fe_2O_3	K_2O	MgO	MnO	Na_2O	P_2O_5	TiO_2	Loss on ignition at 950 °C	Total
(%)	**36,76**	**11,33**	**17,20**	4,40	1,99	2,01	0,05	<0.01	0,17	0,62	20,51	95,04

3.1.2 X-ray diffraction & FTIR analysis

X-ray diffraction (XRD) and Fourier-transform infrared spectroscopy (FTIR) were discussed in the previous study[22]. In brief, X-ray diffraction revealed good crystallinity in the material, with a mineralogical composition dominated by calcite ($CaCO_3$) and quartz (SiO_2). This result was confirmed by XRF, which indicates high SiO_2 and CaO content, suggesting the presence of calcium silicates, which could result from the interaction between the carbonate and silicate phases. Furthermore, infrared spectroscopy shows the presence of absorption bands confirming the presence of carbonates (notably via the ν3 and ν2 vibrations of CO_3^{2-} at 1428 and 870 cm^{-1}), quartz and silicates (ν Si-O and δ Si-O bands around 1007 cm^{-1} and 795–791 cm^{-1}), as well as structural hydroxyl groups (O-H at 3622 cm^{-1}) associated with the octahedral aluminum layers [22].

3.1.3 Textural characterization & Physical and chemical properties

Textural characterization has already been addressed in our previous work [22]: nitrogen adsorption-desorption at 77 K showed isotherms between types III and IV, with an H3-type hysteresis loop (P/P0 > 0.45), typical of a stacked clay forming aggregates of non-uniform particles or slit pores. The BET specific surface area of the calcite-quartz clay is 31.5698 m²/g, its total micropore volume is 0.012279 cm³/g, and its mean pore radius (DH method) is 17.2032 nm. These results confirm the presence of multilayers and capillary condensation within the mesopores. Furthermore, as previously discussed in other studies, the physicochemical properties of our clay (basic pH of 8.5, negative surface charge, high conductivity of 38.9 mS/cm, and very low organic matter content of 0.5%) confirm an alkaline environment and a high basic buffering capacity, with no significant acidifying influence from organic matter [22].

3.1.4 Thermal analysis study

TGA-TDA analysis was used to monitor the thermal behavior of clay. In particular, it allows the measurement of a sample's mass loss as a function of temperature[23]. **Fig. 1** shows the resulting thermal curve. The thermogram of the calcite-quartz clay reveals two phases of mass loss, corresponding to losses of 3.26% and 16.96% of the initial mass, respectively. The first of these losses, observed between 30 and 100 °C, results from the desorption of water adsorbed onto the surface of the clay particles, bound primarily by Van der Waals forces. The second loss, which occurs at temperatures between 100 and 800 °C, results from the removal of interstitial water (water retained between the layers), followed by the dehydroxylation of the structural OH^- groups present in the clay minerals, as well as the possible decomposition of carbonate impurities. All these phenomena reflect the thermal transformations characteristic of phyllosilicates [24,25]. The TDA curve shows an exothermic peak at 32.4 °C, corresponding to the restructuring of calcite and quartz. It also shows endothermic peaks at 79.6 °C, corresponding to the desorption of adsorbed water, at 475.5 °C, corresponding to the volatilization of interstitial water, at 767.2 °C, corresponding to the degradation of hydroxyl groups, and at 888.9 °C, corresponding to the decomposition of carbonates [26,27].

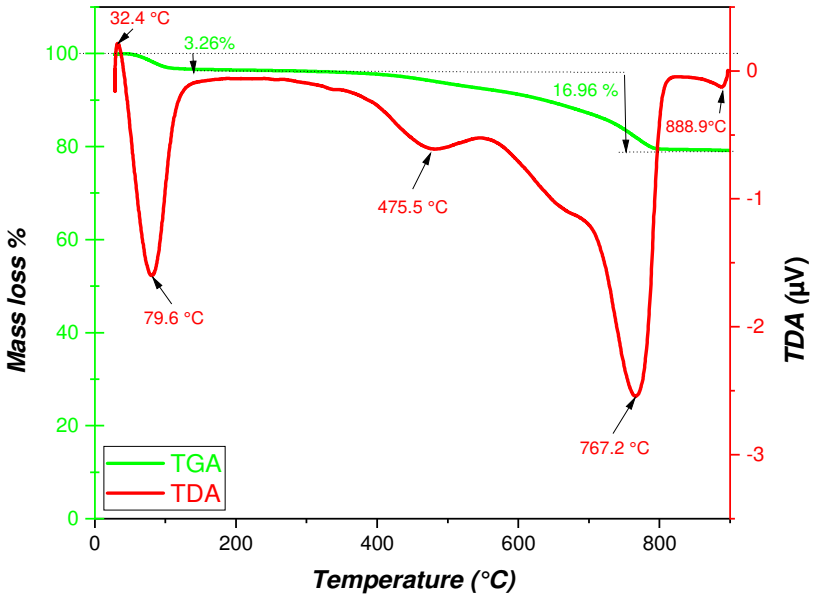

Fig. 1. *TGA-TDA* curves for clay

3.1.5 SEM-EDX analysis

Fig. 2 presents images obtained using scanning electron microscopy at various magnifications.

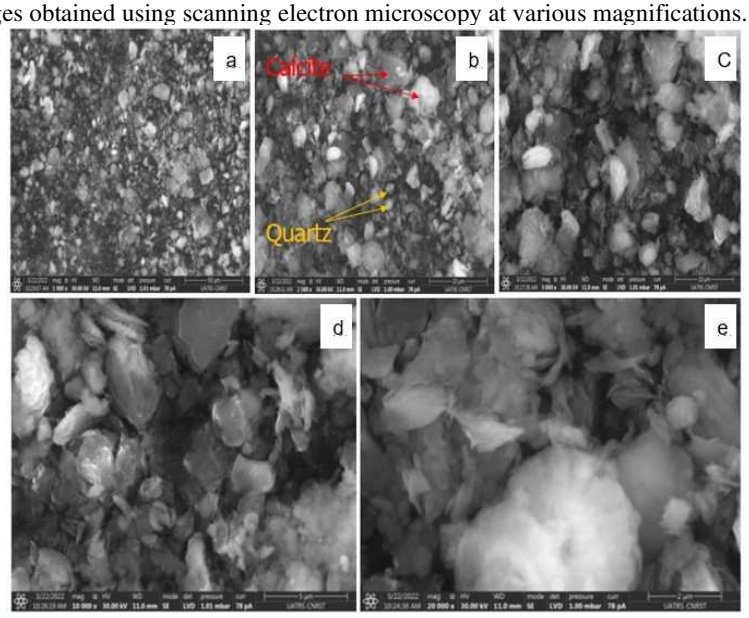

Fig. 2. Scanning electron microscope observations of calcite-quartz clay

According to the SEM results, in the case of calcite-quartz clay, the particles in our sample appear as clusters of small fragments and aggregates with irregular contours [28]. The images confirm the results obtained by XRD, indicating the presence of carbonates (calcite) and quartz in this sample. Indeed, the carbonates (calcite) appear as clearly identifiable aggregates, while the quartz appears as fine grains [28,29]. In addition to SEM analysis, the chemical composition of the calcite-quartz clay sample was determined by EDX analysis. **Table 2** shows the presence of all chemical elements (O, Na, Mg, Al, Si, S, Cl, K, Ca, Fe, Ti). The high silicon content is mainly due to the presence of quartz in this sample. As for the high calcium content, it is due to the presence of calcite.

Table 2. Chemical composition of calcite-quartz clay.

Element	C	O	Na	Mg	Al	Si	S	Cl	K	Ca	Ti	Fe	Total
Weight (%)	10.5	55.24	1.01	1.41	5.43	13.91	0.32	0.23	1.02	8.67	0.36	1.89	100.00
Atom %	16.11	63.64	0.81	1.07	3.71	9.13	0.18	0.12	0.48	3.99	0.14	0.62	100.00

3.2 Adsorption studies

3.2.1 Contact time effect

A study was conducted to investigate the effect of contact time between the adsorbent and the adsorbate in order to determine the time required to reach adsorption equilibrium for Zn^{2+} and Cu^{2+} ions (**Fig. 3**). The experiments were carried out at room temperature (~25 °C), with stirring at 300 rpm and solution volumes of 100 mL.

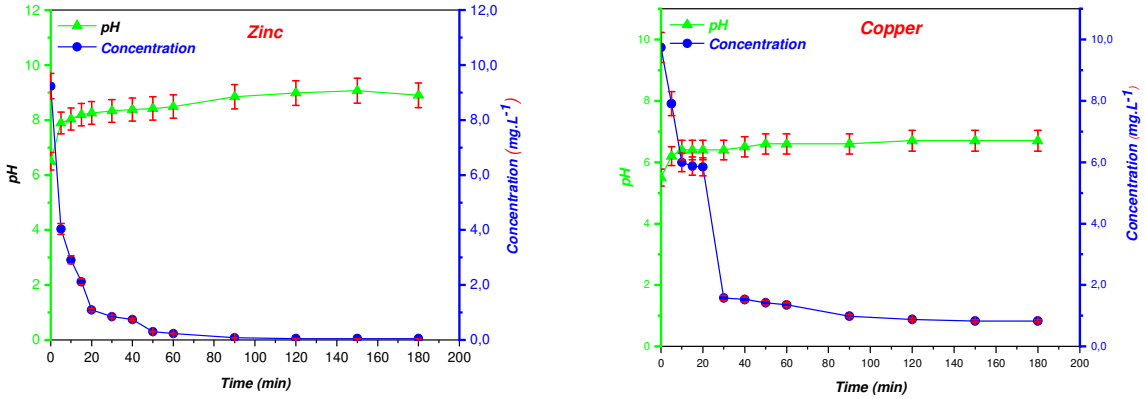

Fig. 3. Variation in Zn and Cu concentration and pH as a function of time

For Zn^{2+}, with an initial concentration of 10 $mg.L^{-1}$ and an initial pH of 6.5, the adsorption kinetics on calcite-quartz clay proceed in three distinct phases: rapid adsorption during the first 20 minutes, followed by a slowing-down phase, and then stabilization at equilibrium. Adsorption equilibrium is reached after 120 minutes, with a maximum capacity of 61.22 $mg.g^{-1}$ and a removal efficiency of 99.46 %. For Cu^{2+}, equilibrium is reached more slowly, after approximately 150 minutes, with a maximum capacity of 59.40 $mg.g^{-1}$ and a removal efficiency of 91.46 %, at an initial pH of 5.5.

The adsorption kinetics of these two metals are characterized first by a rapid initial phase, which can be explained by the high availability of active sites on the clay surface, followed by a gradual slowdown until a plateau is reached. The high adsorption capacity observed is directly related to the density of negatively charged sites on the surface of this calcite-quartz clay. These results confirm the potential of this material for the treatment of liquid effluents containing these metal cations.

3.2.2 Concentration effect

This study analyzed the effect of initial concentrations of Zn^{2+} and Cu^{2+} ions, ranging from 10 to 200 $mg.L^{-1}$, on their adsorption at room temperature over a period of 180 minutes on a clay material. The adsorption kinetics showed a generally similar trend for both metals. As shown in **Fig. 4**, the retention capacities increase with initial concentration and contact time.

When the concentration increases from 10 to 200 $mg.L^{-1}$, the adsorption capacity of Zn by the clay under study increases from 61.22 to 1190 $mg.g^{-1}$, and that of Cu from 59.40 to 672.47 $mg.g^{-1}$. This increase is explained by a greater availability of active sites on the clay's surface, as well as by a stronger driving force pushing ions toward the adsorbent sites at high concentrations, as has been reported in the literature [30].

The results also indicate that the initial concentration of 10 $mg.L^{-1}$ yields optimal removal rates, reaching 99.46 % for Zn^{2+} and 91.46 % for Cu^{2+} with the material under study.

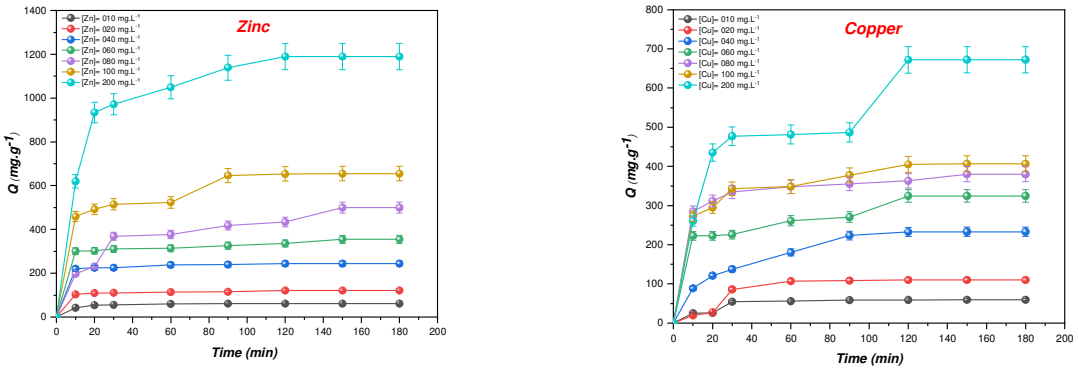

Fig. 4. Evolution of Zn and Cu adsorption at different concentrations as a function of time, (calcite-quartz clay = 0.015 g, V = 100 mL, T= 25 °C)

Table 3. The evolution of clay retention capacity for zinc and copper ions as a function of the concentration changes of these two ions.

Concentration (mg.L^{-1})		10	20	40	60	80	100	200
Zinc	Q_m (mg.g^{-1})	61.22	121.76	243.84	354.53	499.57	655.15	1190
	R (%)	99.46	98.38	98.39	92.33	86.64	85.24	83.80
Copper	Q_m (mg.g^{-1})	59.40	109.92	233.27	324.73	380	406.67	672.47
	R (%)	91.46	90.86	90.81	84.76	70.17	59.67	51.32

3.2.3 Effect of temperature

A thermodynamic analysis was conducted to characterize the nature of the retention processes of Zn^{2+} and Cu^{2+} ions by calcite-quartz clay, at an optimal initial concentration of 10 mg.L^{-1}. The standard thermodynamic parameters : free enthalpy (ΔG°), enthalpy (ΔH°), and entropy (ΔS°), were determined based on experiments conducted under previously defined optimal conditions at temperatures of 25, 35, 45, and 55 °C.

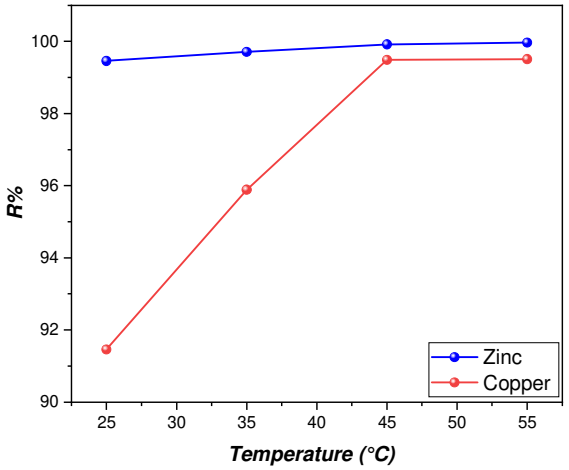

Fig. 5. Variation of the Zn and Cu removal percentage at different temperature values

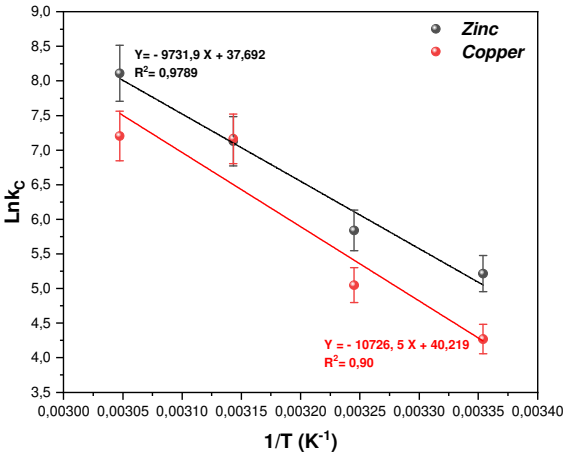

Fig. 6. Adsorption of Zn^{2+} and Cu^{2+} ions - Variation of ln k_C as a function of (1/T)

A comparison of removal efficiencies as a function of temperature (**Fig. 5**) reveals distinct adsorption behaviors for the two metals:

Table 4. Thermodynamic parameters for Zn^{2+} and Cu^{2+} ion adsorption on the clay under study.

	T (°C)	Kc	ΔG° (Kj.mol^{-1})	ΔH° (J.mol^{-1})	ΔS° (J.mol^{-1}.K^{-1})	R^2
Zinc	25	184,19	-12,47	80911	313,37	0.98
	35	343,83	-15,60			
	45	1249	-18,74			
	55	3332,33	-21,87			
Copper	25	71,43	-10.53	90.79	0.34	0.84
	35	155,68	-13.93			
	45	1292,13	-17.33			
	55	1346,25	-20.73			

For zinc, adsorption appears to be virtually independent of temperature. The removal efficiency remains very high and stable, rising only from 99.46 % at 25 °C to 99.97 % at 55 °C, a negligible change of approximately 0.51 %. However, the efficiency of copper adsorption increases significantly as the temperature rises. This indicates that the retention of Cu^{2+} ions on the clay is an endothermic process. This interpretation was confirmed by a thermodynamic analysis. The curves showing the variation of $Ln(k_c)$ as a function of 1/T (**Fig. 6**) allow us to calculate the parameters listed in **Table 4**. Based on these results, the adsorption of zinc and copper onto the clay was found to be a spontaneous ($\Delta G° < 0$) and endothermic ($\Delta H° > 0$) process across the entire temperature range studied. The change in entropy ($\Delta S°$) was positive, indicating an increase in the internal entropy of the system. This phenomenon is most likely due to the release of coordination water molecules when metal ions adsorb onto the surface of the clay studied.

3.3 Adsorption kinetics

A kinetic analysis of the adsorption of Zn^{2+} and Cu^{2+} ions onto calcite-quartz clay was performed by applying standard models to the experimental data[31], using an optimal concentration of 10 $mg.L^{-1}$ for each ion.

3.3.1 Pseudo-first-order and pseudo-second-order kinetic models

To select the model that best describes the adsorption kinetics of Zn^{2+} and Cu^{2+} ions, their linearized forms are compared with the data. Their fit is evaluated by comparing the theoretical adsorption capacities, correlation coefficients, and kinetic parameters derived from each model[32] (**Fig. 7**).

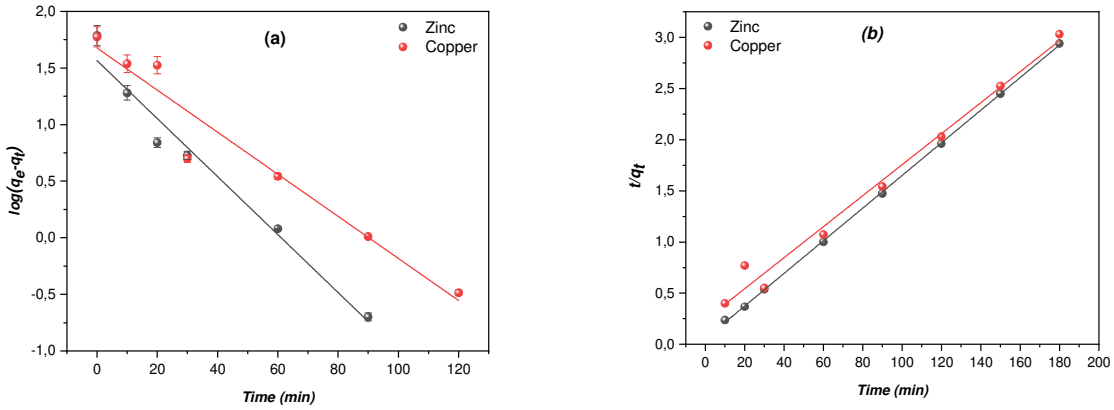

Fig. 7. Linear representations of the kinetic models of (a) pseudo-first order and (b) pseudo-second order for the adsorption of Zn^{2+} and Cu^{2+} ions on the calcite-quartz clay studied

The kinetic results show that the pseudo-second-order model is the most appropriate for modeling the adsorption of Zn^{2+} and Cu^{2+} ions on the clay material. This conclusion is based on two main observations: first, the theoretical curves correspond remarkably well to the experimental data, with extremely high coefficients of determination ($R^2 \approx 1$); On the other hand, the equilibrium adsorption capacity values derived from the model (q_e(calc)) are in close agreement with those measured experimentally (q_e(exp)). The slight differences observed (**Table 5**) confirm that the overall kinetics of the process follow a pseudo-second-order mechanism, in good agreement with the work of Kasbaji et al. (2026) [33].

Table 5. Parameters of pseudo-first-order and pseudo-second-order kinetic models for the adsorption of Zn^{2+} and Cu^{2+} ions.

	q_{exp} (mg g^{-1})	Pseudo first-order model			Pseudo second-order model		
		q_e (mg g^{-1})	K_1 (min^{-1})	R^2	q_e (mg g^{-1})	K_2 (g/mg min)	R^2
Zn	61.22	36.78	0.056	0.97	62.70	0.46×10^{-2}	0.999
Cu	59.40	47.48	0.041	0.93	66.01	0.95×10^{-3}	0.984

3.3.2 Elovich

The Elovich model was used to analyze the experimental data. Table 6 presents the kinetic parameters obtained from this model.

Table 6. The Elovich model parameters.

	Q_{exp} ($mg.g^{-1}$)	α ($mg.g^{-1}.h^{-1}$)	β ($g.mg^{-1}$)	R^2
Zinc	61.22	2.1×10^{3}	0.17	0.78
Copper	59.40	11.02	0.078	0.742

The low correlation coefficient (R^2) observed indicates that the kinetic results obtained using the Elovich model for the adsorption of Zn^{2+} and Cu^{2+} ions by calcite-quartz clay show a significant discrepancy[29]. These results suggest that the model does not adequately describe the adsorption mechanisms at play, which are likely more complex.

3.3 Isotherm studies

3.4.1 Langmuir

Table 7 presents the parameters obtained by applying the Langmuir isotherm to the experimental data on the adsorption of zinc and copper ions by calcite-quartz clay. These parameters reveal certain differences between the two metals. The coefficient of determination (R^2) for zinc ions was 0.80, indicating that the model describes the experimental data fairly well. However, this result suggests that the Zn^{2+} adsorption process in this material may be subject to additional mechanisms and interactions that cannot be fully explained within the simplified assumptions of the Langmuir model[34]. On the other hand, copper adsorption is better explained by this model. In fact, an excellent correlation coefficient (R^2 = 0.935) is observed. Furthermore, the theoretical maximum adsorption capacity calculated by this model (q_{max}(cal) = 714.286 mg·g^{-1}) agrees very well with the experimentally determined value (q_{max}(exp) = 672.47 mg·g^{-1}). Since these two indicator, namely a high R^2 value and the good agreement between the calculated maximum adsorption capacity and the experimental value, are consistent, it can be concluded that the Langmuir model satisfactorily describes the adsorption of Cu^{2+} ions on the surface of the clay under study, which is consistent with the findings of Kasbaji et al. (2026)[33].

Table 7. Langmuir model parameters.

	$q_{m(exp)}$	q_m	K_L	R^2
Zn	1190	1111,11	0,17	0.80
Cu	672.47	714,29	0,077	0.935

3.4.2 Freundlich

The parameters summarized in **Table 8** were obtained by applying the Freundlich isotherm model to the experimental data on the adsorption of Zn^{2+} and Cu^{2+} ions by the clay under study.

Table 8. Freundlich model parameters.

	k_F	n	R^2
Zn	219,97	2,424	0,964
Cu	90,251	2,187	0,910

These results show that the adsorption capacity constant K_F is significantly higher for zinc (219.97) than for copper (90.25). This indicates that the adsorbent has a stronger affinity for zinc, resulting in a higher adsorption capacity at equal concentrations. For both of these metals, the n-coefficient, which indicates adsorption efficiency and capacity, is greater than 1 (2.424 for zinc; 2.187 for copper), confirming the favorable adsorption of these metals on heterogeneous surfaces. Furthermore, the strong correlation observed between zinc and copper (Zn: 0.964 and Cu: 0.910) confirms that the Freundlich model is well-suited to describe this phenomenon. This supports the hypothesis of heterogeneous adsorption and the possibility of multiple adsorption layers.

3.4.3 Temkin

Table 9 presents the results obtained using the Temkin model. These results show that the adsorption capacity for Zn^{2+} is high compared to that for Cu^{2+}, with a Qm value of 1190 mg.g^{-1}. Furthermore, the high value of the Temkin constant K_T for zinc indicates a strong affinity for the surface of this clay adsorbent. In contrast, the higher value of the parameter b corresponding to copper suggests a strong energetic interaction. However, this model fits the experimental data much better for copper (R^2 = 0.930) than for zinc (R^2 = 0.750), suggesting that this model is more appropriate for describing the adsorption of Cu^{2+}.

Table 9. 1Temkin model parameters.

	$Q_{m\ (exp)}$	k_T (L.mg^{-1})	b (J.mol^{-1})	R^2
Zinc	1190	11,14	17,82	0.750
Copper	672.47	1,770	21,792	0,930

4. Conclusion

This study evaluated the adsorption capacity of a natural Moroccan clay composed of quartz and calcite, collected in the Sidi Kacem region, to remove metal ions (Zn^{2+} and Cu^{2+}) from an aqueous solution. Key operational parameters, such as adsorbent mass, contact time, initial metal ion concentration, and temperature, were studied in detail. The results show that optimal removal rates were achieved at an initial concentration of 10 mg.L^{-1}, namely 99.46 % for Zn^{2+} and 91.46 % for Cu^{2+}. These results, when compared to those published in the scientific literature, indicate that this clay is more effective

than other types of natural clays. For example, in a study conducted by Eleraky et al. (2025), the use of activated calcium bentonite resulted in an adsorption capacity of 14 $mg.g^{-1}$ for copper (II) [35], while other studies achieved capacities of up to 131.66 $mg.g^{-1}$ for zinc (II) and 98.15 $mg.g^{-1}$ for copper (II) using mixtures of raw clay (2025) [36]. This comparison shows that the calcite-quartz clay from Sidi Kacem is an excellent natural adsorbent, capable of effectively removing heavy metals without any chemical treatment, making it both an effective and inexpensive material.

The kinetic study of the adsorption of Zn^{2+} and Cu^{2+} ions by the clay in question shows that the pseudo-second-order model best fits the experimental data, with correlation coefficients close to unity and a strong agreement between the theoretical and experimental amounts adsorbed at equilibrium. The analysis of adsorption isotherms shows that the Langmuir, Freundlich, and Temkin models can be used to describe the adsorption of Cu^{2+} on the calcite-quartz clay studied (R^2>0.91), suggesting adsorption on both homogeneous and heterogeneous surfaces. In contrast, Zn^{2+} adsorption is better described by the Freundlich model (R^2 = 0.964) than by the Langmuir model (R^2 = 0.80), indicating multilayer adsorption on a heterogeneous surface. The maximum adsorption capacities obtained are competitive with those reported for other low-cost natural adsorbents in recent literature.

The thermodynamic study shows that the adsorption of zinc and copper onto the clay under study is spontaneous ($\Delta G° < 0$). The positive values of $\Delta H°$ and $\Delta S°$ indicate that the process is endothermic and suggest an increase in the disorder of the system.

In conclusion, this natural calcite-quartz clay from the Sidi Kacem region is an effective, inexpensive, and locally available adsorbent capable of removing zinc and copper from contaminated water. In the future, research should focus on optimizing operating conditions at the pilot scale, evaluating the regenerability of the adsorbent material, and testing its application on actual industrial effluents, with a view to sustainable implementation in wastewater treatment in Morocco.

Acknowledgements

We would like to express our gratitude to the Center of Excellence in Analysis, Technology, and Transfer at Ibn Tofail University in Kenitra, as well as the National Center for Scientific and Technical Research of Morocco, for giving us access to the scientific equipment of the UATRS division. Our thanks also go to the National Bureau of Hydrocarbons and Mines for their support.

References

1. El Morabet, R., Barhazi, L., Bouhafa, S., Dahim, M. A., Khan, R. A., & Dahim, A. M. (**2024**). Water Quality, Heavy Metal Contamination and Health Risk Assessment of Surface Water Bodies of Mohammedia Prefecture, Morocco. *Environ. Chem. Ecotoxicol.*, 6, 33–41. https://doi.org/10.1016/j.enceco.2023.12.002.
2. Anjum, A., Garg, R., Garg, R., Gupta, D., & Eddy, N. O. (**2025**). Efficient Sequestration of Zinc and Copper from Aqueous Media: Exploring Strategies, Mechanisms, and Challenges. *Int. J. Environ. Sci. Technol.*, 22(6), 5105–5126. https://doi.org/10.1007/s13762-024-06060-2.
3. Cheng, Y., Zhao, Y., Chen, C., & Zhang, F. (**2025**). Heavy Metals Toxicity: Mechanism, Health Effects, and Therapeutic Interventions. *MedComm*, 6(9), e70241. https://doi.org/10.1002/mco2.70241.
4. Fei, Y., & Hu, Y. H. (**2023**). Recent Progress in Removal of Heavy Metals from Wastewater: A Comprehensive Review. *Chemosphere*, 335, 139077. https://doi.org/10.1016/j.chemosphere.2023.139077.
5. Benalla, S., Addar, F. Z., Tahaikt, M., Elmidaoui, A., & Taky, M. (**2022**). Heavy Metals Removal by Ion-Exchange Resin: Experimentation and Optimization by Custom Designs. *Desalination Water Treat.*, 262, 347–358. https://doi.org/10.5004/dwt.2022.28607.
6. Khulbe, K. C., & Matsuura, T. (**2018**). Removal of Heavy Metals and Pollutants by Membrane Adsorption Techniques. *Appl. Water Sci.*, 8(1), 19. https://doi.org/10.1007/s13201-018-0661-6.
7. Hussain, A., Madan, S., & Madan, R. (**2021**). Removal of Heavy Metals from Wastewater by Adsorption. In Khaled Nazal, M., & Zhao, H. (Eds.), *Heavy Metals - Their Environmental Impacts and Mitigation*. IntechOpen. https://doi.org/10.5772/intechopen.95841.
8. Vedenyapina, M. D., Kurmysheva, A. Yu., Kulaishin, S. A., & Kryazhev, Yu. G. (**2021**). Adsorption of Heavy Metals on Activated Carbons (A Review). *Solid Fuel Chem.*, 55(2), 83–104. https://doi.org/10.3103/S0361521921020099.
9. Mambetova, M., Dossumov, K., Baikhamurova, M., & Yergaziyeva, G. (**2024**). Sorbents Based on Natural Zeolites for Carbon Dioxide Capture and Removal of Heavy Metals from Wastewater: Current Progress and Future Opportunities. *Processes*, 12(10), 2071. https://doi.org/10.3390/pr12102071.
10. Gu, S., Kang, X., Wang, L., Lichtfouse, E., & Wang, C. (**2019**). Clay Mineral Adsorbents for Heavy Metal Removal from Wastewater: A Review. *Environ. Chem. Lett.*, 17(2), 629–654. https://doi.org/10.1007/s10311-018-0813-9.
11. El Kerdoudi, Z., Bensalah, J., Ferraa, N., El Mekkaoui, A., Berisha, A., Safi, Z., Ouaddari, H., Khallouki, F., Dauelbait, M., Nafidi, H.-A., Z. Gaafar, A.-R., Bourhia, M., Habsaoui, A., & Mejdoub, N. E. (**2023**). Physicochemical Characterization of Clay and Study of Cationic Methylene Blue Dye Adsorption. *ACS Omega*, 8(43), 40848–40863. https://doi.org/10.1021/acsomega.3c06019.

12. Chen, T., Cao, G., Qiang, Y., Lu, Y., Qin, R., Xu, W., Xie, Y., & Mao, R. (**2024**). Effective Removal of Pb (II) from Wastewater by Zinc-Iron Bimetallic Oxide-Modified Walnut Shell Biochar: A Combined Experimental and DFT Calculation Approach. *J. Environ. Manage.*, 370, 122757. https://doi.org/10.1016/j.jenvman.2024.122757.
13. Wang, J., & Guo, X. (**2020**). Adsorption Kinetic Models: Physical Meanings, Applications, and Solving Methods. *J. Hazard. Mater.*, 390, 122156. https://doi.org/10.1016/j.jhazmat.2020.122156.
14. Vashishtha, M., & Kumar, K. V. (**2026**). Insights into Solid–Liquid Adsorption Kinetics: Theory, Mechanisms, and Practical Guidelines. *ACS EST Water*, 6(5), 2569–2601. https://doi.org/10.1021/acsestwater.5c00497.
15. Mohan, S., Ashwini, K., & Dinesha, P. (**2025**). CO_2 Uptake on Fruit Wastes-Derived Activated Hydrochars: Systematic Modeling of Adsorption Kinetics and Isotherms. *Sci. Rep.*, 16(1), 205. https://doi.org/10.1038/s41598-025-30726-7.
16. Zangi, R. (**2024**). Breakdown of Langmuir Adsorption Isotherm in Small Closed Systems. *Langmuir*, 40(7), 3900–3910. https://doi.org/10.1021/acs.langmuir.3c03894.
17. Danat, B. T., Wuana, R. A., Chahul, H. F., & Iorungwa, M. S. (**2026**). Review of Adsorption Isotherms Models. *Appl. Water Sci.*, 16(3), 72. https://doi.org/10.1007/s13201-025-02682-0.
18. Bensalah, J., Berradi, M., Habsaoui, A., Allaoui, M., Essebaai, H., El Khattabi, O., Lebkiri, A., & Rifi, E.-H. (**2021**). Kinetic and Thermodynamic Study of the Adsorption of Cationic Dyes by the Cationic Artificial Resin Amberlite®IRC50. *Mater. Today Proc.*, 45, 7468–7472. https://doi.org/10.1016/j.matpr.2021.02.028.
19. Esmaeili Nasrabadi, A., Babaei, N., & Bonyadi, Z. (**2025**). Effect of Ozonation on the Morphological Characteristics and Adsorption Behavior of Polystyrene Microplastics in Aqueous Environments. *Appl. Water Sci.*, 15(5), 90. https://doi.org/10.1007/s13201-025-02443-z.
20. Di Remigio, G., Rocchi, I., & Zania, V. (**2021**). Scanning Electron Microscopy and Clay Geomaterials: From Sample Preparation to Fabric Orientation Quantification. *Appl. Clay Sci.*, 214, 106249. https://doi.org/10.1016/j.clay.2021.106249.
21. Raghdi, A., Heraiz, M., Rasheed, M., & Keziz, A. (**2024**). Investigation of Halloysite Thermal Decomposition through Differential Thermal Analysis (DTA): Mechanism and Kinetics Assessment. *J. Indian Chem. Soc.*, 101(11), 101413. https://doi.org/10.1016/j.jics.2024.101413.
22. Kerdoudi, Z. E., Bensalah, J., Rhilassi, A. E., Laabaissi, T., Ferraa, N., El Meskini, I., Mazzah, A., Zarrouk, A., & Mejdoub, N. E. (**2026**). Comparative Adsorption of Methylene Blue on Quartz Clay and Calcite-Quartz Clay from Morocco: Overview Based on Kinetics, Isotherms, and Surface Characterization. *Euro-Mediterr. J. Environ. Integr.*, 11(4), 154. https://doi.org/10.1007/s41207-026-01121-z.
23. Bousemat, H., Ziane-Hezil, S., Benatmane, S., Bessaha, F., Bessaha, G., Çoruh, A., Sillanpää, M., & Khan, M. A. (**2025**). Experimental and Modeling Studies for the Simultaneous Removal Anionic Dyes in Single and Binary Systems Using Activated Clay. *Sci. Rep.*, 15(1), 45512. https://doi.org/10.1038/s41598-025-30039-9.
24. Lo Dico, G., Lisuzzo, L., Carcelén, V., Cavallaro, G., & Haranczyk, M. (**2024**). Thermogravimetric Analysis of Moisture in Natural and Thermally Treated Clay Materials. *Materials*, 17(10), 2231. https://doi.org/10.3390/ma17102231.
25. Polcowñuk Iriarte, I. A., Mocciaro, A., Rendtorff, N. M., & Richard, D. (**2025**). Dehydroxylation of Kaolinite: Evaluation of Activation Energy by Thermogravimetric Analysis and Density Functional Theory Insights. *Minerals*, 15(6), 607. https://doi.org/10.3390/min15060607.
26. Tassongwa, B., Eba, F., Njoya, D., Tchakounté, J. N., Jeudong, N., Nkoumbou, C., & Njopwouo, D. (**2017**). Physico-Chemistry and Geochemistry of Balengou Clay Deposit (West Cameroon) with Inference to an Argillic Hydrothermal Alteration. *Comptes Rendus Géoscience*, 349(5), 212–222. https://doi.org/10.1016/j.crte.2017.06.002.
27. Moctar, I. B., Yannick, T. L., Albertine, A. S.-T., Mache, J. R., & Mominou, N. (**2023**). Physico-Chemical, Mineralogical Characterization, and Ceramic Properties of Clay Materials from South Mindif (Far North, Cameroon). *JMST Adv.*, 5(1), 13–26. https://doi.org/10.1007/s42791-023-00047-9.
28. Hussein, A. F., Al-Bidry, M. A., & Wasiti, A. A. A. (**2025**). Investigation and Evaluation of Palygorskite Microstructure Following Acid Pretreatment and Its Potential Use as an Adsorbent for Copper. *Sci. Rep.*, 15(1), 3813. https://doi.org/10.1038/s41598-025-88449-8.
29. Kanzaoui, M. E., Hajjaji, A., Guenbour, A., & Boussen, R. (**2018**). Development and Study of Mechanical Behaviour Reinforcing Composites by Waste BTP. *MATEC Web Conf.*, 149, 02012. https://doi.org/10.1051/matecconf/201814902012.
30. El-Sayed, G. O., Sedek, S. A., & Abdallah, N. M. (**2017**). Removal of Cu (II) and Zn (II) Ions from Aqueous Solution by Clay Mineral. *J. Basic Environ. Sci.*, 4(2), 140–148. https://doi.org/10.21608/jbes.2017.369653.
31. Al-Labadi, I. G., Horváth, M., Alkilani, A. T., Al-Ma'abreh, A. M., Bashir, M. J. K., Keshta, B. E., Hanbali, G., Al Zoubi, W., Abukhadra, M. R., Alqhtani, H. A., & Eid, M. H. (**2025**). Simultaneous Adsorptive Removal of Pb^{2+}, Cd^{2+}, Cu^{2+}, and Zn^{2+} Using Raw Norway Spruce Biomass: A Low-Cost and Eco-Friendly Solution for Wastewater Treatment. *Front. Water*, 7, 1612232. https://doi.org/10.3389/frwa.2025.1612232.
32. Azanfire, B.-E., Bulgariu, D., Cimpoeşu, N., & Bulgariu, L. (**2025**). Efficient Removal of Toxic Heavy Metals on Kaolinite-Based Clay: Adsorption Characteristics, Mechanism and Applicability Perspectives. *Water*, 17(13), 1938. https://doi.org/10.3390/w17131938.
33. Kasbaji, M. A., Kasbaji, M., El Wafi, O., Hafdi, A., M'Barki, M., El Achaby, M., & Oubenali, M. (**2026**). Experimental and Theoretical Analysis of Single- and Binary-System Cationic-Anionic Dye Adsorption onto Magnetic Lignin-Alginate Beads. *Sep. Purif. Technol.*, 394, 137430. https://doi.org/10.1016/j.seppur.2026.137430.

34. Rhilassi, A. E., & Ziatni, M. B. (**2023**). Studies of Kinetic Models and Adsorption Isotherms: Application on the Interaction of Insulin with Synthetic Hydroxyapatite. *Curr. Chem. Lett.*, 12(2), 445–458. https://doi.org/10.5267/j.ccl.2022.11.001.
35. Eleraky, M. I., Razek, T. M. A., Hasani, I. W., & Fahim, Y. A. (**2025**). Adsorptive Removal of Lead, Copper, and Nickel Using Natural and Activated Egyptian Calcium Bentonite Clay. *Sci. Rep.*, 15(1), 13050. https://doi.org/10.1038/s41598-025-95184-7.
36. Houmia, I., Fardioui, M., Amri, A. E., Houmia, B., Kaibous, N., Bazhar, K., Hammani, O., Arhoutane, M. R., & Guedira, T. (**2025**). Structural Characterization and Ecological Evaluation of Natural Clay Mixtures for the Removal of Heavy Metals (Cu(II), Co(II), and Zn(II)) from Aqueous Solutions: Experimental Study Combined with RSM Process Optimization. *J. Mol. Struct.*, 1344, 142917. https://doi.org/10.1016/j.molstruc.2025.142917.

© 2026 by the authors; licensee Growing Science, Canada. This is an open access article distributed under the terms and conditions of the Creative Commons Attribution (CC-BY) license (http://creativecommons.org/licenses/by/4.0/).